Boundary-Layer Meteorol (2006) 121:537–556
DOI 10.1007/s10546-006-9080-6

ORIGINAL PAPER

Role of shear and the inversion strength during sunset turbulence over land: characteristic length scales

David Pino · Harm J. J. Jonker · Jordi Vilà-Guerau de Arellano · Alessandro Dosio

Received: 15 July 2005 / Accepted: 3 April 2006 /
Published online: 22 June 2006

Abstract The role of shear and inversion strength on the decay of convective turbulence during sunset over land is systematically studied by means of large-eddy simulations. Different decay rates have been found for the vertical and horizontal velocity fluctuations, resulting in an increase of the anisotropy for all the studied cases. Entrainment, which persists during the decay process, favours the appearance of vertical upward movements associated with a conversion from kinetic to potential energy. Particular attention is paid to the evolution of the characteristic length scale of the various turbulent variables during this process. The length scale evolution is found to depend on the wind shear characteristics, but not on the strength of the inversion. In general the length scales of the variables grow during decay because small-scale fluctuations dissipate faster than large-scale fluctuations. Only the length scale of the vertical velocity component remains nearly constant during decay. Spectral analysis of the variance budgets shows that pressure correlations are responsible for fixing this length scale, effectively compensating the strong but oscillating influence of buoyancy. In the shear cases, after an initial period of growth, the length scales start to decrease once the buoyancy-generated variance has sufficiently subsided. Also here the effect of pressure redistribution is crucial, as it transfers the spectral influence of shear to the other velocity components.

D. Pino (✉)
Applied Physics Department, Technical University of Catalonia and Institute for Space Studies of Catalonia (IEEC/CSIC), Barcelona, Spain
e-mail: david@fa.upc.edu

H. J. J. Jonker
Department of Multi–Scale Physics, Delft University of Technology, Delft, The Netherlands

J. Vilà-Guerau de Arellano · A. Dosio
Meteorology and Air Quality Section, Wageningen University, Wageningen, The Netherlands

A. Dosio
Atmospheric Sciences Section. Centre for Ecology and Hydrology (CEH), Edinburgh, UK

Keywords Characteristic length scales · Convective turbulence · Demixing · Turbulence decay

1 Introduction

Near sunset, the surface heat flux progressively decreases and, consequently, the convective eddies that maintain turbulence start to loose their strength, and the convective turbulence in the boundary layer begins to decay. Several authors have previously studied this transition regime of atmospheric turbulence. Through laboratory experiments, Monin and Yaglom (1975) studied the decay of grid-generated turbulence under neutral conditions. During the decay, the turbulence maintains the initial isotropy, with the energy decay following a power law t^{-n}, t being time. Cole and Fernando (1993), by performing an experiment in a water tank, studied the decay of temperature and velocity fluctuations in a convective turbulent boundary layer in response to cooling at the surface. They found that, when the cooling rate is constant, the decay times of turbulent velocity and temperature fields scale with a time that is proportional to the temperature difference between the cooling surface and the mixed-layer temperature, and inversely proportional to the cooling rate. Stillinger et al. (1983) studied the decay of homogeneous turbulence in a uniform stratification showing that turbulence becomes highly anisotropic. On the other hand, turbulence decay has been also studied by using theoretical models (George 1992), large-eddy simulation models (LES) (Touil at al. 2002) or direct numerical simulations (DNS) (Biferal et al. 2003). Specifically, atmospheric transitional boundary layers have been much less studied than quasi-stationary situations such as the convective and stable boundary layers. The convective turbulence decay in the atmospheric boundary layer has been analyzed by Goulart et al (2003) using theoretical models; by Nieuwstadt and Brost (1986) (hereafter NB86), Sorbjan (1997) and Goulart et al. (2003) by means of LES; and recently Shaw and Barnard (2002) used DNS to study the same problem. Moreover, Caughey and Kaimal (1977), Grant (1997), Acevedo and Fitzjarrald (2001), Grimsdell and Angevine (2002), Anfossi et al. (2004) and recently Fitzjarrald et al. (2004) reported some observations and in some cases compared these with LES results.

Our study builds on these previous works by studying specifically the role played by the inversion strength and shear during the decay of convective turbulence. Particular effort is addressed towards understanding the evolution of the characteristic length scales of the turbulent variables during this process. Our study attempts to complete the previous numerical work of NB86, who, by means of LES, analyzed an idealized case of the decay of turbulence with constant geostrophic wind ($5\,\mathrm{m\,s^{-1}}$) and different inversion strength, $\Delta\Theta_v$, mean virtual potential temperature in the mixed layer, Θ_{vm}, and boundary-layer depth, h, at the beginning of the turbulence decay. Time evolution of the volume averaged variables, vertical profiles and convection patterns were compared in order to determine which processes are relevant during the decay. For one of their cases, they found a different behaviour in the decay of turbulence characterized by the return to equilibrium levels of warm air parcels, i.e., a 'demixing' process. Recently, Grimsdell and Angevine (2002) by means of wind profiler observations and radiosondes postulated two types of afternoon transition of the convective boundary layer and related them to the

two types of decay process, with or without the demixing process, described by NB86.

Compared to the previous studies, we attempt to study systematically the role of external forcing and fluxes in the entrainment zone during sunset turbulence. First, the roles of the shear and of the inversion strength are studied by maintaining other variables, such as boundary-layer depth or bulk temperature, similar between the different simulations during the decay of convective turbulence. Our aim is to analyze how these external forcings act to maintain turbulence in the boundary-layer evening transition. Notice that, currently, the majority of numerical models with boundary-layer schemes do not represent specifically this transition. Therefore, by performing this study, we attempt to obtain information of the relevant scaling variables and spatial/temporal characteristic scales essential in deriving future representations of the evening transition. Second, due to the improvement of computer facilities, higher resolution and larger domains are prescribed. Finally, we focus on the evolution of characteristic length scales during the decay of a dry convective boundary layer. Only Grant (1997) dealt with this aspect intensively. He calculated the spectra of the vertical velocity component at different times and heights during an observational campaign during August 1990 at Cardington, England, and found that during the decay process the spectral peak of the vertical velocity spectra in the boundary layer shifts to smaller length scales. By using LES, NB86 and Goulart et al. (2003) found that the position of the spectral peak of the vertical velocity variance remains constant during their simulations. In contrast, Sorbjan (1997) showed some evidence that the spectral peak of the vertical velocity variance shifts toward larger eddies, i.e., the larger eddies decay slower than the smaller ones. Because of the disparity of these previous results, we attempt to clarify the evolution of the characteristic length scale during the decay of turbulence.

The simulations will be presented in Sect. 2, and in Sect. 3 the time evolution of the turbulent variables and the evolution of their characteristic length scales will be shown. Sect. 4 summarizes the results.

2 Numerical set-up

The LES model is described in Cuijpers and Duynkerke (1993) and has been modified by Cuijpers and Holtslag (1998). In the simulations, different wind profiles and inversion strengths are prescribed. Each of the four decay experiments begins with a fully developed dry convective boundary layer, which has been generated by heating the surface for 2 h at a constant rate ($\overline{w\theta_0} = 0.1\,\mathrm{K\,m\,s^{-1}}$, $\overline{wq_0} = 0$), where the overbar denotes time average. At this moment (t_0), the surface heat flux is set to 0, 2 h more were simulated, and the statistics were calculated every 2 min. It is important to note that, despite this situation occurring in reality only during an eclipse, the inclusion of a smooth decay of the surface heat flux, which better simulates sunset conditions, does not introduce any particular differences with the cases considered here (Sorbjan 1997). The simulated domain was in all the cases $12.8 \times 12.8 \times 2.048\,\mathrm{km^3}$ with grid spacing $\Delta x = \Delta y = 50\,\mathrm{m}$ and $\Delta z = 16\,\mathrm{m}$. This resolution is high enough to correctly simulate a convective boundary layer (Pino et al. 2003) and a neutrally stratified boundary layer (Andren et al. 1994).

The differences between the four runs are only based on the inversion strengths and mean winds prescribed. Regarding the shear characteristics, two different boundary

layers were considered. A pure buoyancy–driven boundary layer, without geostrophic winds, namely NS (no shear), and a boundary layer driven both by buoyancy and shear (SH, shear), where the geostrophic wind is constant with height, being its components in the x and y direction at the beginning of the simulation $U_g = 10\,\mathrm{m\,s^{-1}}$, and $V_g = 0\,\mathrm{m\,s^{-1}}$, respectively. Regarding the virtual potential temperature jump at the inversion, the initial mean potential temperature for all the simulations was 306 K below 888 m. Depending on the inversion case considered, it increases 1 K for the weak inversion cases, or 5 K for the strong inversion case, across one Δz grid level, and finally increases with a constant rate of $3\,\mathrm{K\,km^{-1}}$ until it reaches the top of the domain. It is important to note that a strong inversion jump equates, to some extent, to a rigid lid at the interface, but differs obviously with regard to the behaviour and influence of the entrainment flux. Simulations with a rigid lid could be useful to further isolate the inversion interactions from the other processes, but are not considered here. Table 1 shows the initial values of the inversion strength and wind characteristics for the four simulations performed.

3 Results

The vertical profiles of virtual potential temperature and virtual potential temperature flux for all the cases, and the vertical profile of horizontal velocity component in the x direction, U, for the shear cases after two simulated hours, just before the decay process starts (t_0), are presented in Fig. 1. At this moment all the simulated CBLs are in steady state, i.e., the boundary-layer averaged turbulent kinetic energy (TKE) is approximately constant. As can be observed in Fig, 1a, b, the differences in the vertical profiles between the cases are mainly due to the inversion strength, i.e., shear does not introduce large differences in virtual potential temperature or virtual potential temperature flux after 2 h. In Fig. 1c the effect produced by the inversion strength in the mean wind in the x direction can also be observed.

Table 2 shows the main flow characteristics for all the simulations. In the Table, the Richardson number is defined as (Pino et al. 2003):

$$Ri = \frac{gh}{\Theta_{vm}} \frac{\Delta\Theta_v}{w_m^2}, \tag{1}$$

$$w_m^3 = w_*^3 + 8u_*^3, \tag{2}$$

where g is the gravity constant, and u_*, w_* are the friction and convective velocities, respectively.

From the Table, it is clear that the four cases can be separated depending on the value of h and u_*. We attempted to combine these two variables in the defined Richardson number in order to explain the different behaviour in the decay process. As will be shown, Ri is not the only parameter to characterize the decay process.

Table 1 Initial values of the inversion strength and wind profile in the x direction for the studied cases

	NS1	NS5	SH1	SH5
$\Delta\Theta_v$ (K)	1	5	1	5
U_g ($\mathrm{m\,s^{-1}}$)	0	0	10	10

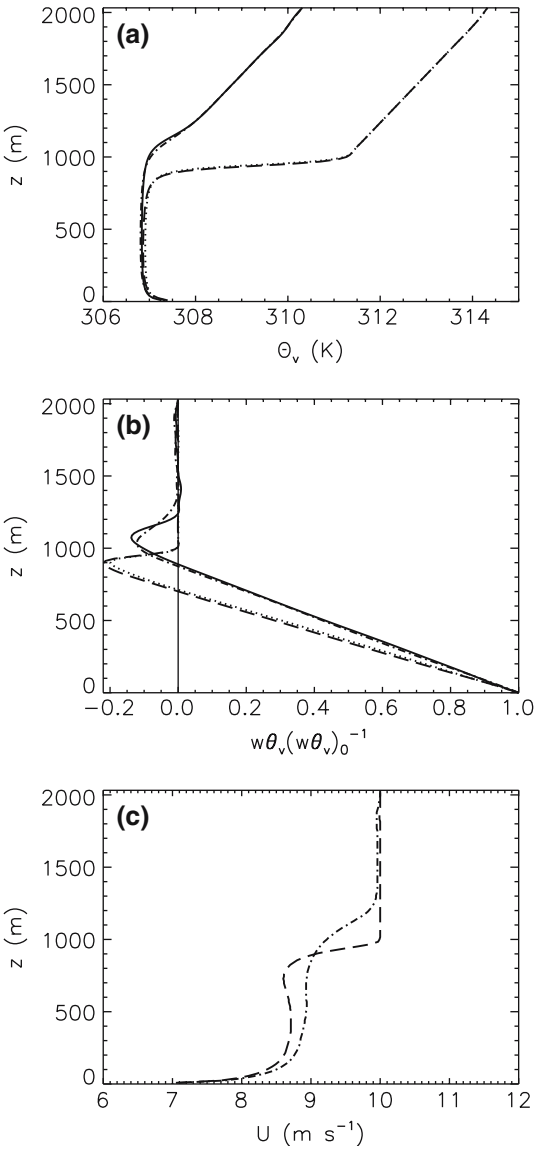

Fig. 1 (**a**) Vertical profiles of the virtual potential temperature, (**b**) of the virtual potential temperature flux, and (**c**) of the U component of the mean wind for the shear cases after 2 h of simulation, before the decay of turbulence begins for NS1 (solid line), NS5 (dotted line), SH1 (dashed–dotted line) and the SH5 (dashed line) simulations

Following NB86, who showed that decay of turbulence is self-similar with respect the dimensionless time $tw_m h^{-1}$, we have used h/w_m and w_m^2 to nondimensionalize time and velocity variances respectively. It is important to notice that NB86 did not use w_m but w_*, which does not include the surface shear characteristics. By doing this, as the values for w_m and h presented in Table 2 vary for each case, different $tw_m h^{-1}$ values are obtained for each case at the same time t.

Table 2 Boundary-layer variables and scaling parameters at the beginning of the decay process for each simulation. h is the height where the virtual potential temperature gradient is maximum, z_i is the height of the minimum buoyancy flux, $\Delta\Theta_v = \Theta_v(h) - \Theta_{vm}$, $\Delta U = U(h) - U_m$, where U_m is the value of the horizontal velocity component in the x direction at the middle of the boundary layer, and the rest of the variables are defined in the text

	NS1	NS5	SH1	SH5
Θ_{vm} (K)	307.1	307.6	307.1	307.7
h (m)	1160	952	1044	936
z_i (m)	1072	896	1040	896
$\Delta\Theta_v$ (K)	0.68	2.69	0.68	2.18
w_* (m s^{-1})	1.54	1.44	1.54	1.44
u_* (m s^{-1})	10^{-4}	10^{-4}	0.44	0.44
ΔU (m s^{-1})	0.031	0.014	1.01	1.03
Ri	10.6	39	9.4	27

3.1 TKE and variances time evolution

Figure 2 shows for all the studied cases the turbulent kinetic energy, horizontally averaged and over the boundary layer and normalized by means of w_m^2, as a function of tw_mh^{-1}. As shown for all the studied cases, the TKE remains constant and the curves collapse onto a single curve during one eddy turnover time (around 15 min). Therefore, the breakdown of the convective boundary layer occurs rapidly, as noted by Kaimal et al. (1976) and Caughey and Kaimal (1977) who described observations for the afternoon transition. After $tw_mh^{-1} \approx 1$, similarity is not fulfilled and NS and SH cases present different decay evolution, decaying faster for the NS simulations. The exponent of the power law for the NS case at the beginning of the decay is similar to the unique exponent that NB86 found ($n = -1.2$) in all of their shear simulations. The shear cases present higher exponents that are similar to the simulation D−1 of Sorbjan (1997), who did not suddenly shut–off the surface heat flux, but decreased it with time. Then, it is clear that the exponent of the power law of TKE in the decay process depends on the contribution of shear to the maintenance of atmospheric turbulence. If NS cases are considered, a strong inversion tends to slightly slow down the turbulence decay. For 3D homogeneous isotropic turbulence, George (1992) showed that the decay rate has a power–law form with an exponent that depends on the initial conditions, so that the decay rate constants cannot be universal. Chasnov (1994) pointed out that, within these conditions, the exponent of the decay process is always lower than −1. By using LES in the same conditions, Touil et al. (2002) reproduced the helium superfluid experiment of Skrbek and Stalp (2000) and found an exponent $n = -2$ for the decay of the TKE in a bounded domain.

In order to study the behaviour of the components of the TKE, Fig. 3 shows the evolution of the resolved velocity variances averaged horizontally and over the boundary layer, $0.5\left\langle\overline{u^2}\right\rangle$, $0.5\left\langle\overline{v^2}\right\rangle$ and $0.5\left\langle\overline{w^2}\right\rangle$, normalized by means of w_m^2 as a function of tw_mh^{-1} (the angular brackets denote a domain average). As can be observed a vertical shift appears for $0.5\left\langle\overline{u^2}\right\rangle$ and the curves do not collapse for $tw_mh^{-1} < 1$. This fact is due to the different contributions of shear for the simulations. The decay of this velocity variance can be approximately described by a power law with exponent $n \approx -1$ only for the NS cases; SH cases decay slowly. Furthermore, by comparing NS1

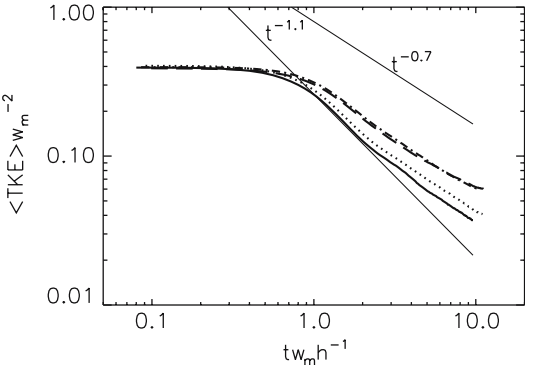

Fig. 2 Volume-averaged (from $z = 0$ to $z = h$) turbulent kinetic energy (TKE) and nondimensionalized by w_m^2 as a function of tw_mh^{-1} for the NS1 (solid line), NS5 (dotted line), SH1 (dashed–dotted line) and the SH5 (dashed line) simulations. The thin lines serve as a guide to the eye to give an indication of the decay rates

and NS5 evolution, or SH1 and SH5, one can conclude that strong inversion strength only slightly decelerates the decay process of this variance.

Regarding the evolution of $0.5\left\langle \overline{v^2} \right\rangle$, except for a small vertical shift, the same evolution is observed for all the cases. Notice that no flow was initially prescribed in this direction. For this component of the velocity and due to the small flow in this direction, all the cases can be approximately described by a power law with exponent $n \approx -1$,

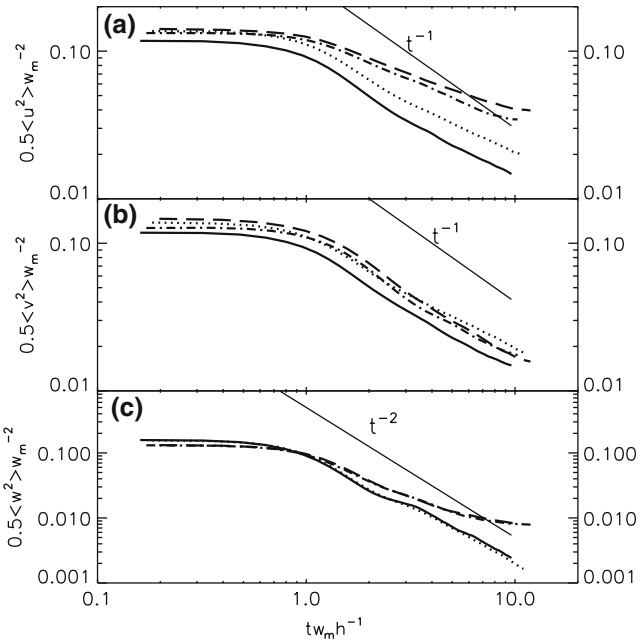

Fig. 3 One half of the volume-averaged (from $z = 0$ to $z = h$) resolved velocity variances, $\left\langle \overline{u^2} \right\rangle$ (**a**), $\left\langle \overline{v^2} \right\rangle$ (**b**), and $\left\langle \overline{w^2} \right\rangle$ (**c**), and nondimensionalized by w_m^2 as a function of tw_mh^{-1} for the NS1 (solid line), NS5 (dotted line), SH1 (dashed–dotted line) and the SH5 (dashed line) simulations. The thin lines serve as a guide to the eye to give an indication of the decay rates

i.e., for the variance of this velocity component there is no difference between NS and SH simulations.

As with $\left\langle \overline{u^2} \right\rangle$, the presence of shear makes the volume–averaged vertical velocity variance decay with a different slope (Fig. 3c). Conversely, inversion strength does not play any role on the decay of the vertical velocity variance. NS and SH cases collapse almost onto a single curve for $tw_m h^{-1} < 1$. The decay process for NS can be approximately reproduced by a power law with exponent -2. For the SH cases, the exponent is larger and is not constant with time. For a decay process with a confined outer length scale, like the vertical velocity variance bounded by the boundary-layer depth, h, a power law with an exponent $n \approx -2$ is expected (Tennekes and Lumley 1972; Touil et al. 2002). However, the length scales of the horizontal velocity variances, which are only confined by the domain size, can grow unbounded, implying an exponent $n > -2$ (e.g., NB86). The different decay profile of the horizontal and vertical velocity variances has been also observed in the real atmosphere (Fitzjarrald et al. 2004). In this work, six cases of the evening transition from convective to stable boundary layers were observed by means of flux towers and aircraft measurements. They clearly observed a decay in the w variance, though the u, v variances decreased more slowly or even increased for some of the nights. For these specific nights, TKE does not present a clear decrease in its behaviour. Therefore, the differences in the exponent of the variances of the three components of the velocity is a clear indication that the turbulence does not relax to an isotropic state during the decay process. On the contrary, the anisotropy increases during the decay of convective turbulence.

To determine the evolution of the anisotropy on the decay of the velocity variances, we calculated it according to $\left(\left\langle \overline{u^2} \right\rangle + \left\langle \overline{v^2} \right\rangle\right) \left(2\left\langle \overline{w^2} \right\rangle\right)^{-1}$ (Fig. 4). At the beginning of the decay process, the two simulations with shear present an almost perfect isotropy, NS simulations are much more anisotropic in the vertical direction, especially NS1. For $tw_m h^{-1} \gtrsim 1$, the anisotropy grows for all the cases. However, the growth rate depends on time, i.e., the exponent of the power laws that represent the decay process is not constant. For one of the cases (NS1), and to a lesser extent NS5, between $2 \lesssim tw_m h^{-1} \lesssim 3.5$, the horizontal profile of the anisotropy is characterized by a large increase of $\left\langle \overline{w^2} \right\rangle$, which was also found by NB86 for one of their simulations. This increase occurs in flows with a weak inversion and almost no shear. The shear cases have a tendency to an asymptotic value after $tw_m h^{-1} = 3$. In all cases, turbulence does not relax to an isotropic state.

The variance of temperature averaged across the boundary layer (Fig. 5) begins to decay almost immediately and all the cases reveal a different time evolution. This may be due to the fact that temperature variance is dominated by near-surface production. Due to the larger $\left\langle \overline{\theta^2} \right\rangle$ in the entrainment zone, the strong inversion cases present larger values of $\left\langle \overline{\theta^2} \right\rangle$ and decay slower than the NS1 and SH1 cases.

3.2 Vertical profiles

The vertical profile of the buoyancy flux provides one of the keys to understanding the decay process. Figure 6 shows the time evolution of the virtual potential temperature flux vertical profile for the four simulated cases. The virtual potential temperature flux evolution is as follows for all the cases. At the beginning of the process, the heat flux

at the surface becomes zero but at higher levels it remains positive until $t \approx 18$ min (Fig. 6b). During this period, the averaged TKE in the boundary layer is constant (Fig. 2) and a positive lapse rate appears in the boundary layer. This fact was observed by Grant (1997) during several boundary-layer evening transitions. Fig. 7b shows the vertical profile of the virtual potential temperature gradient, where the stable stratification in the boundary layer can be observed. This stratification plays a key role in the decay of convective turbulence (Cole and Fernando 1993). After this time, as entrainment takes place continuously, a negative virtual potential temperature flux is found throughout the whole boundary layer (Fig. 6c). This process was observed by Kaimal et al. (1976) during the evening transition of a real convective boundary layer. For $30 \lesssim t \lesssim 50$ min, all the cases show a reverse in the flux sign, and a positive buoyancy flux in the boundary layer (Fig. 6d). During this period a large increase of $\left\langle \overline{w^2} \right\rangle$ occurs, which is also reflected in the constant anisotropy of the NS1 case between $2 < tw_m h^{-1} < 3$ (see Fig. 4). However, differences can be observed between the cases. NS5, which is the case with low entrainment rates due the large inversion strength and no shear, presents the lowest values of the positive virtual potential temperature flux.

In the NS5, SH1, and SH5 cases the virtual potential temperature flux turns negative and tends to zero. However, for NS1 it turns to positive for $66 < t < 80$ min (Fig. 6e).

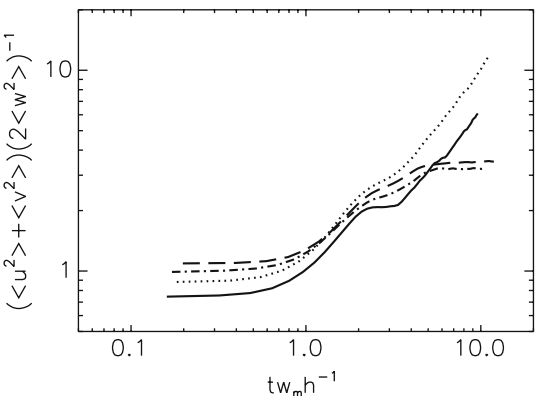

Fig. 4 Anisotropy as a function of $tw_m h^{-1}$ for the NS1 (solid line), NS5 (dotted line), SH1 (dashed–dotted line), and the SH5 (dashed line) simulations

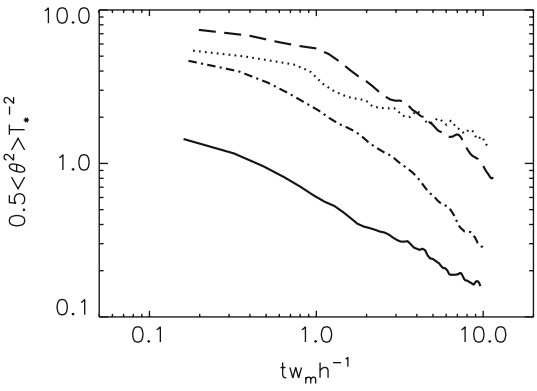

Fig. 5 One half of the volume-averaged (from $z = 0$ to $z = h$) resolved temperature variance nondimensionalized by T_*^2, where $T_* = \overline{w\theta_0}/w_m$, as a function of $tw_m h^{-1}$ for the NS1 (solid line), NS5 (dotted line), SH1 (dashed–dotted line) and the SH5 (dashed line) simulations

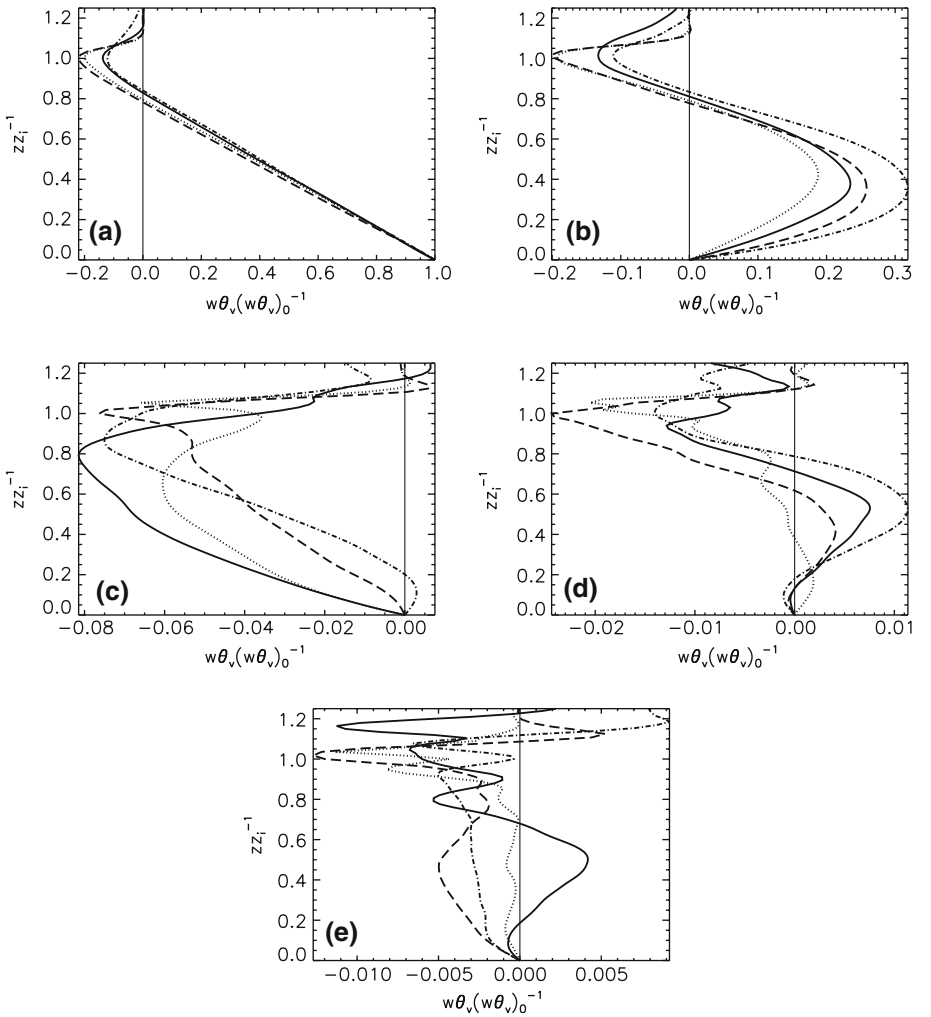

Fig. 6 Buoyancy flux nondimensionalized by its initial surface value as a function of zz_i^{-1} at 0 (**a**), 8 (**b**), 18 (**c**), 36 (**d**), and 72 (**e**) min during the decay process for the NS1 (solid line), NS5 (dotted line), SH1 (dashed–dotted line), and the SH5 (dashed line) simulations

The evolution of the virtual potential temperature flux shown above determines the evolution of the potential temperature profile. Figure 7 shows the vertical profile of the virtual potential temperature (left) and of the virtual potential temperature gradient (right) 16 min after the cut-off in the surface flux. For all the studied cases, due to the positive gradient of the virtual potential temperature flux in the lower part of the boundary layer (Fig. 6b), temperature decreases. Afterwards ($t \approx 14$ min), as the upper part of the boundary layer continues to warm, a positive gradient of the virtual potential temperature can be found throughout the boundary layer (Fig. 7b). This positive gradient does not change during the rest of the decay process and implies a downward transport of heat. Therefore, the remaining large coherent eddies of the former convective boundary layer lose energy gradually.

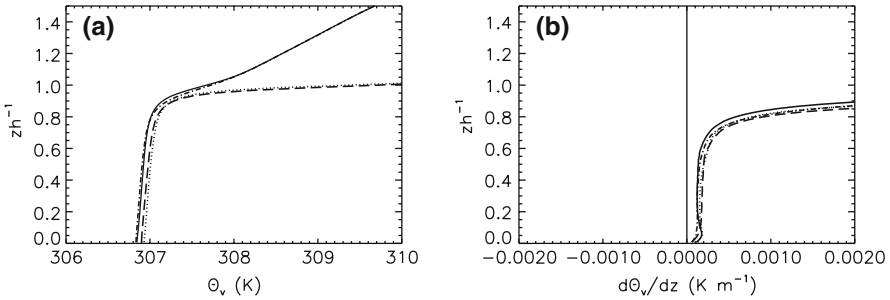

Fig. 7 Virtual potential temperature (**a**) and virtual potential temperature gradient (**b**) as a function of zh^{-1} at 16 min after the beginning of the decay for the NS1 (solid line), NS5 (dotted line), SH1 (dashed–dotted line), and the SH5 (dashed line) simulations

The oscillating behaviour in the virtual potential temperature flux was observed by Caughey and Kaimal (1977) and Grimsdell and Angevine (2002) and it is similar to one of the studied numerical experiments of NB86. They termed it 'demixing' and is associated with cycles in the conversion between kinetic and potential energy. In short, when small-scale turbulence has almost dissipated shortly after t_0, temperature fluctuations are not mixed, and warm air coming from the free troposphere can move downward until large-scale turbulence has lost all its energy. Then, these parcels that are warmer than the environment, tend to return to their equilibrium levels, moving upward. This fact is clearly marked by the positive buoyancy flux at the middle of the boundary layer shown in Figs. 6d, e.

NB86 concluded that the appearance of demixing in a sheared convective boundary layer is dependent on the strength of the inversion. Very large $\Delta\Theta_v$ will prevent entrainment and consequently the production of temperature fluctuations. However, in their study they did not analyze situations with large $\Delta\Theta_v$ and moreover, they only found demixing effects for the experiment with the largest inversion strength ($\Delta\Theta_v = 2$ K). With respect to the study of NB86, two important aspects need to be discussed. First, the definition of $\Delta\Theta_v$ as used by NB86 is unclear. If they used a similar definition to the one used in our study, their inversion strengths were comparable to the two cases considered here. Second, in their simulations, other variables apart from inversion strength, such as, Θ_v and h, should be considered to explain why there is no demixing for the experiments with the smallest inversion strength. In other words, as the inversion strength is not the only parameter that varies between the experiments of NB86, it is difficult to determine the role played by the inversion strength in the 'demixing' process. In NB86, the initial surface heat flux is different for each simulation, consequently the mean temperature in the boundary layer, Θ_{vm}, is also different. Then, it is difficult to extract the influence of the inversion strength on the demixing effects. In our numerical experiments, where we only vary $\Delta\Theta_v$ and u_*, we find demixing effects for all the studied cases: NS1 and SH1 with small inversion strength, SH5 characterized by a large inversion strength with shear and also for NS5 with a large inversion and no shear. However, for the latter the demixing effects, i.e., the magnitude of the positive virtual potential temperature flux associated with warm lumps of air moving upwards in the middle of the boundary layer once the decay process has started, are not so important. Moreover, by observing Table 2, one can conclude that low *Ri* favours demixing, and its effects lose intensity with increasing *Ri*.

In summary, besides the inversion strength, the presence of shear at the surface and at the inversion, which enhances the entrainment fluxes (Tennekes and Driedonks 1981; Fedorovich et al. 2001; Pino et al. 2003), as a consequence favours the strength of demixing events.

3.3 Characteristic length scales

A main objective of this research is to study the evolution of the characteristic length scales of the turbulence variables during the decay of convective turbulence. By doing this, the role played by the different processes that control the decay of convective turbulence is better understood, and therefore, one might improve the form of parametric expressions of the transition boundary layer after sunset.

By calculating the 2D spectra of the LES results, we estimate the evolution of the characteristic length scales during the decay of convective turbulence. We focus on the spectra determined in the middle of the boundary layer, obtained at $t = 2, 20, 40,$ and 80 min after the beginning of the decay process. Figure 8 shows for NS1 the $\overline{w^2}$, $\overline{u^2}$ and $\overline{\theta^2}$ spectra at $zh^{-1} = 0.5$ normalized by σ^2/k, where σ^2 is the corresponding variance and k is the wavenumber. This normalization ensures that the area under all spectral curves amounts to unity, which greatly facilitates the comparison between spectra taken at different times during the decay process. An additional advantage of plotting spectra on log–linear axes is that a peak in the spectra can be interpreted as the wavenumber that has the largest relative contribution to the variance.

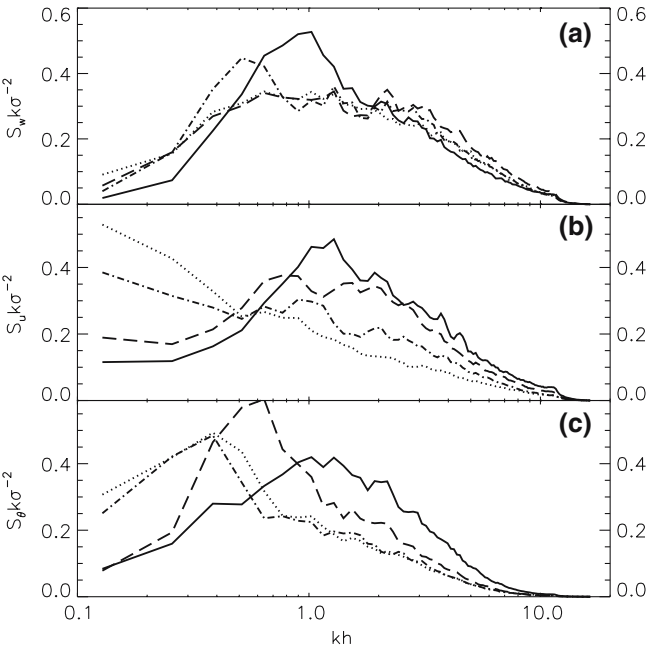

Fig. 8 Spectral density at the middle of the boundary layer ($zh^{-1} \approx 0.5$) of $\overline{w^2}$ (**a**), $\overline{u^2}$ (**b**) and $\overline{\theta^2}$ (**c**) normalized by σ^2/k, where σ^2 denotes the variance of the studied variable, for $t = 2$ (solid), 20 (dashed), 40 (dash–dotted), and 80 min (dotted) for NS1 ($tw_m h^{-1} = 0.16$, 1.6, 3.2, and 6.4, respectively)

At the selected times, the vertical profile of the virtual potential temperature flux has the following characteristics: (a) it is positive in the boundary layer just after the beginning of the decay ($t = 2$ min, $tw_m h^{-1} = 0.159$), (b) it is negative in the whole boundary layer ($t = 20$ min, $tw_m h^{-1} = 1.59$), (c) it is positive in the middle of the boundary layer ($t = 40$ min, $tw_m h^{-1} = 3.19$), and (d) it has very small negative values ($t = 80$ min, $tw_m h^{-1} = 6.37$).

As can be observed in Fig. 8a, the position of the spectral peak of the vertical velocity variance remains near h, except for $t = 40$ min when it slightly shifts to lower wavenumbers. At this moment, NS1 has a positive virtual potential temperature flux in the middle of the boundary layer due to a demixing event. Once the demixing event is over ($t = 80$ min), the peak returns roughly to its original value.

A more spectacular and consistent shift of the spectral peak can be observed in the spectra of $\overline{u^2}$, shown in Fig. 8b. During the decay there is a drastic shift to larger scales, such that at the end of the simulation the largest contribution to the variance of $\overline{u^2}$ originates from the largest possible simulated scales. This means that fluctuations with a length scale of the order of the lateral domain size dominate the variance. A similar evolution can be observed in the spectra of $\overline{v^2}$ (not shown here). Finally, the spectra of $\overline{\theta^2}$ (Fig. 8c) show a behaviour comparable to the spectra of u and v, although the effect is less pronounced.

To provide a comprehensive overview of the spectral behaviour during the decay of the different variables in the different cases, we present in Fig. 9 the evolution of the characteristic length scales derived from the spectra. Several definitions have been proposed in order to define a characteristic length scale (Λ), one obvious choice being the wavenumber at which the spectral peak is located, but this method is often found to suffer from the erratic behaviour of the peak, which is a natural consequence of the turbulent process (e.g., Jonker et al. 2004). A length scale based on a weighted integral of the spectrum is therefore more favourable in this respect (e.g., De Roode et al. 2004). In the present study, the characteristic length scale of a variable ψ is defined as follows:

$$\Lambda_\psi^{-a} = \frac{\int_0^\infty S_\psi(k) k^a dk}{\int_0^\infty S_\psi(k) dk}, \quad a \neq 0, \tag{3}$$

where $S_\psi(k)$ is the spectral density of the variance of ψ for each wavenumber k averaged over the entire simulated domain, i.e.: $\int_0^\infty S_\psi(k) dk \approx \left\langle \overline{\psi^2} \right\rangle$. By considering the characteristic length scale across the whole domain, and not only in the middle of the boundary layer, we include all the turbulence effects that can affect the characteristic length scale. For instance, shear is mainly present at the surface and across the inversion layer. Note that the choice of the parameter a in (3) influences the way in which the small and large scales are weighted. We consider the choice of $a = 1$ as used by Jonker et al. (1999) not ideal, since too much weight is exerted on the small scales – for example, a $k^{-5/3}$ spectrum multiplied by k yields a divergent integral, showing the importance of spectral shape at the smallest resolved scale. As we are interested in the large-scale range (of the order h and larger), we use in the present study $a = -1$ (e.g., Pope 2000; Jonker and Vilà-Guerau de Arellano 2005).

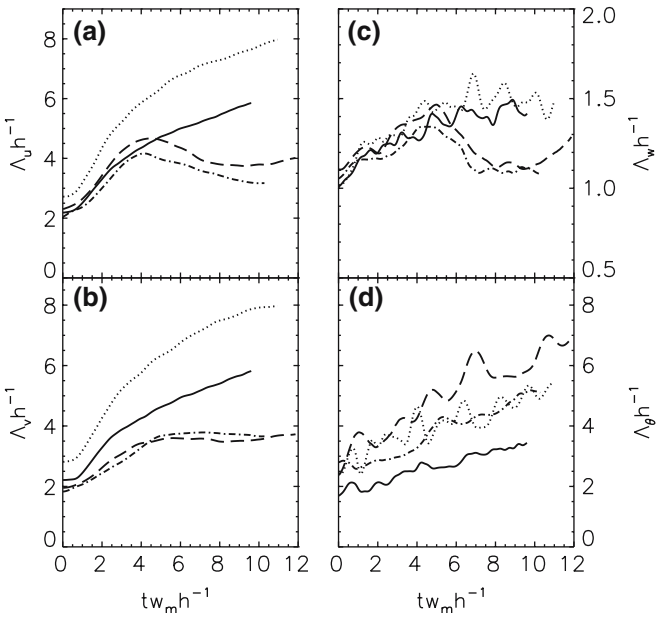

Fig. 9 Time evolution of characteristic length scale Λ averaged across the whole domain of u (**a**), v (**b**), w (**c**), and θ (**d**) as a function of $tw_m h^{-1}$ for NS1 (solid), NS5 (dotted), SH1 (dashed–dotted), and SH5 (dashed)

Figure 9 shows the time evolution of the characteristic length scales of u, v, w, and θ as a function of $tw_m h^{-1}$ for all the simulated cases. On the basis of this figure we can draw the following conclusions:

(a) The length scales of u and v reveal a strong increase during the decay process. Only in the case of shear, this growth is halted after a while, and the length scales start to decrease.
(b) The length scale of w changes only marginally and remains roughly equal to the depth of the boundary layer.
(c) The length scale of θ increases rather persistently, also in the shear cases.
(d) The strength of the inversion has only a small influence on the evolution of the characteristic length scales, since the behaviour of SH1 largely resembles that of SH5, and the behaviour NS1 resembles that of NS5 – at least in a qualitative sense.

To understand these results it is useful to make a comparison with decaying homogeneous and isotropic turbulence and highlight both the similarities and the differences. In the theory of decaying homogeneous and isotropic turbulence the length scale of a variable ψ is usually taken as (e.g., Tennekes and Lumley 1972):

$$\Lambda_\psi = \frac{\left(\overline{\psi^2}\right)^{3/2}}{\epsilon_\psi}, \tag{4}$$

where $\overline{\psi^2}$ is the variance of ψ and ϵ_ψ is the variance loss by dissipation. A decay law of $\overline{\psi^2} \sim t^{-n}$, and $\epsilon_\psi = -\partial\overline{\psi^2}/\partial t \sim t^{-n-1}$ results in the following evolution for the length scale

$$\Lambda_\psi \sim t^{(2-n)/2}. \tag{5}$$

For homogeneous isotropic decay, the reported exponents typically vary between $n = 1.1$ and 1.5, implying that the length scale Λ_ψ must grow in time; this also indicates that the small eddies decay faster than the large eddies.

However, if the decaying turbulence is somehow confined in space, for example due to the presence of outer boundaries, it is clear that Λ_ψ cannot grow indefinitely and must approach a limiting *constant* value. Equation (5) then implies that the decay exponent must become $n = 2$ (e.g., Tennekes and Lumley 1972; Touil et al. 2002).

From these theoretical/empirical considerations one can understand the behaviour of the u and v length scales during decay, at least in the no-shear situations. Since u and v can then decay freely, and since the outer boundaries will not be felt for a long period, the length scales Λ_u and Λ_v are expected to grow at least until the lateral domain size is reached (e.g., Touil et al. 2002). As to the w length scale, since the vertical extent of eddies is confined by the boundary-layer depth, the length scale of w is limited. This result is consistent with (5) because the observed decay exponent for the w variance (Fig. 3) was $n \approx 2$ in the no-shear cases.

The preceding arguments do not pay attention to the roles of buoyancy and shear. To sketch a more comprehensive picture it is useful to consider the variance budget equations (e.g., Stull 1988):

$$\frac{\partial}{\partial t}\left\langle \overline{u^2} \right\rangle = \frac{2}{\overline{\rho}}\left\langle \overline{p\frac{\partial u}{\partial x}} \right\rangle - 2\left\langle \overline{uw}\frac{\partial U}{\partial z} \right\rangle - \epsilon_u, \tag{6}$$

$$\frac{\partial}{\partial t}\left\langle \overline{v^2} \right\rangle = \frac{2}{\overline{\rho}}\left\langle \overline{p\frac{\partial v}{\partial y}} \right\rangle - \epsilon_v, \tag{7}$$

$$\frac{\partial}{\partial t}\left\langle \overline{w^2} \right\rangle = \frac{2}{\overline{\rho}}\left\langle \overline{p\frac{\partial w}{\partial z}} \right\rangle + \frac{2g}{\Theta_m}\left\langle \overline{w\theta} \right\rangle - \epsilon_w, \tag{8}$$

where $\overline{\rho}$ is the mean density, p is the pressure, and $\epsilon_\psi = 2\nu\left\langle \overline{(\partial\psi/\partial x_j)^2} \right\rangle$ represents the dissipation terms for the variables $\psi = u, v, w$. Besides dissipation, Eqs. 6–8 show the relevance of three terms: (1) the shear-production term $-2\langle \overline{uw}\,\partial U/\partial z \rangle$ (only relevant for the equation of the u variance budget in the cases SH1 and SH5), (2) the buoyancy-production term $2g\left\langle \overline{w\theta} \right\rangle/\Theta_m$, and (3) the pressure-correlation terms.

We have studied the spectral decompositions of Eqs. 6–8 to assess the relative importance of each term at different scales. We will avoid here the technical details of such analyses (see e.g., Domaradzki and Rogallo 1989), and only briefly discuss the main conclusions:

(a) *Shear production*. The shear–production term displays a spectral peak at length scales between 200 m and 300 m. This means that shear imposes its own length scale, which is significantly smaller than the boundary-layer depth h. Yet during the first period of the decay the shear generated variance is not strong enough to leave a fingerprint in the spectrum. Only during the later stages of the decay ($tw_m h^{-1} \gtrsim 5$), when the buoyancy-generated variance gradually has diminished, does shear become significant and its impact becomes noticeable in the length scale evolution shown in Fig. 9. If the runs were integrated for a longer period, we anticipate that the velocity length scales eventually converge to the shear-imposed length scale.

(b) *Buoyancy production*. In all cases studied (NS and SH), buoyancy production was found to be a significant term in the variance budget. But since the buoyancy flux frequently changes sign during the decay (see Fig. 6), the effect of the buoyancy–production term on the length-scale evolution is not consistent, as it can enhance as well as inhibit the growth of Λ_w. The net effect can only be well understood by accounting for the pressure-correlation term, discussed next.

(c) *Pressure correlation*. In all the cases studied this term was found to be of major importance, both in the variance budget and in the length-scale evolution. For instance, in the $\langle\overline{w^2}\rangle$ spectral budget the strong but oscillating contribution from the buoyancy-production term is invariably compensated by the pressure-correlation term $\langle\overline{p\,\partial w/\partial z}\rangle$, which also oscillates but with opposing phase. In consequence, the action of pressure ensures that the length scale of w remains nearly constant, even though buoyancy production alternatively enhances and inhibits the growth of Λ_w.

In the shear cases, the pressure-correlation term is also markedly present in the spectral budgets when the buoyancy-generated variance has sufficiently decayed ($tw_m h^{-1} \gtrsim 5$). A significant amount of the shear production in the $\langle\overline{u^2}\rangle$ budget is then consumed by $\langle\overline{p\,\partial u/\partial x}\rangle$, and fed back into the v and w components via $\langle\overline{p\,\partial v/\partial y}\rangle$ and $\langle\overline{p\,\partial w/\partial z}\rangle$, an effect known as pressure redistribution (the sum of the three terms must always vanish). This explains, for example, why the length-scale evolution of v mimics that of u even though there is only a marginal amount of direct shear production in v. For this case, the effect of shear via pressure redistribution becomes also visible in Λ_w after $tw_m h^{-1} = 5$.

In summary, the growth of Λ_u, Λ_v in the no-shear cases and the growth of Λ_θ in all cases can be well understood from the analogy with decaying isotropic turbulence: the small-scale fluctuations decay faster than the large-scale fluctuations. It is important to stress the difference between this mechanism for increasing length scales, and the mechanisms identified in studies of the non-decaying turbulent atmospheric boundary layer (e.g., Müller and Chlond 1996; Dörnbrack 1997; Jonker et al. 1999; and De Roode et al. 2004). Also we emphasize that the increase of length scales is not due to an upscale spectral transfer of variance. During the evolution of the turbulence decay, the variance at large scales is surely decreasing, yet the length scale based on the weighted spectrum integral increases because the variance at small scales just decreases faster. The spectra depicted in Fig. 8 are deceiving in this respect, owing to the normalization by the total variance. The same effect can be observed in instantaneous horizontal cross-sections of horizontal velocity fluctuations in the middle of the boundary layer (Fig. 10); this gives the impression that the size of the spatial structures increases during the decay, because in fact the smaller structures have disappeared.

Finally, the behaviour of Λ_w can be understood through the confinement of vertical structures by the CBL depth h, and was found to be consistent with the predicted decay exponent for the vertical velocity variance by Eq. (5). In the spectral budget of $\langle\overline{w^2}\rangle$, the action of pressure was identified as responsible for fixing the length scale of w during decay, effectively compensating the significant influence of buoyancy. We note in passing that since the pressure term is found in a temporal sense to be "locked" to the buoyancy term, it displays the same temporal characteristics. This behaviour contrasts for example with the observations under stationary stable conditions conducted

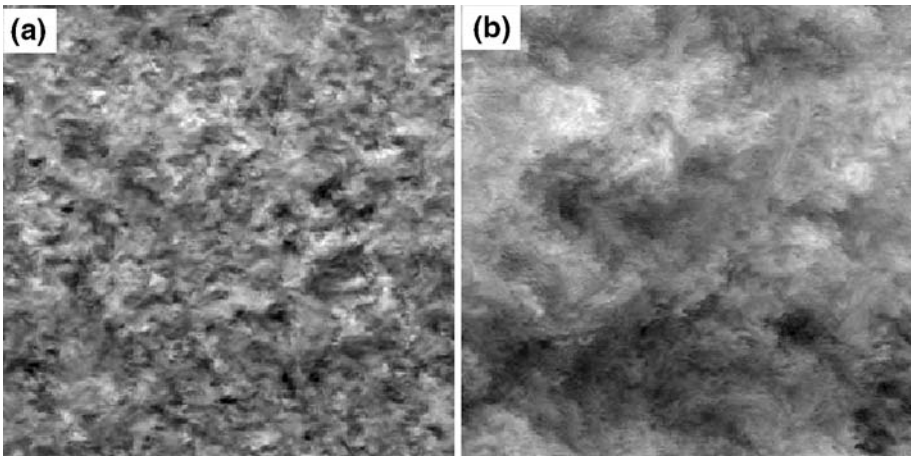

Fig. 10 Horizontal cross-sections in the $x - y$ plane of the horizontal velocity in the x direction at $zh^{-1} \approx 0.5$ of NS1 at 2 min (**a**), and 120 min (**b**) after the beginning of the decay process

by Cuxart et al. (2002), who found that the pressure term fluctuated on significantly larger time scales than the other terms in the TKE budget.

4 Conclusions

The influence of the inversion strength and wind shear on the decay of convective turbulence at sunset over land is studied by means of large-eddy simulations. Compared with previous studies, the numerical experiments are done with finer resolution and larger domain size. Sensitivity studies based on different values of external forcing for the geostrophic wind and for the temperature inversion are carried out. The demixing process discussed previously by NB86 appeared for all the simulated cases, and depends on the inversion strength and wind profile characteristics. We have shown that weak inversion strengths and specially wind shear (low Ri at the inversion), which enhance entrainment during the decay of convective turbulence, also favour the demixing.

The volume-averaged TKE remains constant during one eddy turnover time. The TKE evolution scales well using the scaling velocity w_m and the nondimensional time $tw_m h^{-1}$. However, once the TKE starts to decay, the rate of the decay process depends on the importance of the shear contribution. In the case with no shear, turbulence decays faster. Consequently, the decay rate is a function of the flow characteristics (with or without shear). If the variances of the velocity components are considered, we show that the variance of the horizontal components decays much slower than that of the vertical component; therefore anisotropy grows in all cases. This phenomenon has been also observed in the real atmospheric boundary-layer evening transition (Fitzjarrald et al. 2004).

Particular effort is devoted to studying the evolution of the spectra of the main turbulent variables during the decay of turbulence. For all the studied cases, the spectral peak position of the vertical velocity variance remains approximately constant during the decay of turbulence. A weak relationship between demixing events and a shift of the w-spectral peak to larger scales has been found for the no-shear cases.

In the horizontal velocity and temperature variances a large shift of the spectral peak to large scales has been observed for all the cases.

A length-scale definition based on a weighted integral of the spectrum, which avoids the possible fluctuations of the maximum of the spectra, has been used. For all the variables, the inversion strength has a small influence on the evolution of the characteristic length. With respect to the characteristic length scale of the horizontal velocities, we show that Λ_u increases in all the cases at the beginning of the decay process. The growth is not due to an upscale spectral transfer of variance, but results from the fact that small-scale fluctuations dissipate faster than large-scale fluctuations. When shear is not present this process continues until the end of the simulation. For shear cases we find that the influence of the shear term, which imposes a length scale smaller than h, becomes important once the buoyancy-generated variance has sufficiently decayed. From this moment Λ_u decreases with time.

For the no-shear cases the evolution of Λ_v is very similar to that of Λ_u, as was expected. Surprisingly, this also happens when shear is present. This is remarkable, because there is hardly any direct shear production in the v component, and one might have expected a continuous growth of Λ_v such as occurs for the no-shear cases. However, analysis of the spectral variance budgets revealed that shear is indirectly affecting the evolution of Λ_v through redistribution by the pressure term. Therefore, Λ_v stops growing and even decreases once shear effects are dominant in the evolution of Λ_u.

The length scale based on the $\overline{w^2}$ spectra, Λ_w, was found to remain approximately constant with a value near h, specially for no-shear cases. The spectral analysis revealed strong oscillating contributions from buoyancy, but which were nearly always effectively counteracted by the pressure–correlation term, rendering Λ_w virtually unchanged. When SH1 and SH5 cases are considered, the effects of shear become visible through pressure redistribution in the later stages of the decay ($tw_m h^{-1} \gtrsim 5$), reducing the value of Λ_w. Such an effect has been previously observed by e.g., Grant (1997), who observed 3 days with constant boundary-layer winds of about $6\,\mathrm{m\,s^{-1}}$, he found that the spectral peak of the vertical velocity variance shifts to smaller scales.

For all our studied cases, large-scale fluctuations of the horizontal velocities and temperature variances dominate shortly after the decay process begins due to the faster dissipation of the small scales. For the description of the transition from a convective to a stable boundary layer, the constant value of $\Lambda_w \sim h$ during decay suggests, at least during the first stages of decay, to maintain in the prescribed parameterization h as the characteristic length of the process.

Acknowledgements The visits by the first author to the Wageningen University were supported by a UPC mobility grant. This work was sponsored by the Stichting Nationale Computerfaciliteiten (National Computing Facilities Foundation, NCF) with the projects SG-132 and SG-061 for the use of supercomputing facilities, with financial support from the Netherlandse Organisatie voor Wetenschappelijk Onderzoek (Netherlands Organization for Scientific Research, NWO). We thank two anonymous reviewers for comments on an earlier version of the paper.

References

Acevedo OC, Fitzjarrald DR (2001) The early evening surface-layer transition: temporal and spatial variability. J Atmos Sci 58:2650–2667

Andren A, Brown AR, Graf J, Mason PJ, Moeng C-H, Nieuwstadt FTM, Schumann A (1994) Large-Eddy simulation of a neutrally stratified boundary layer: a comparison of four computer codes. Quart J Roy Meteorol Soc 120:1457–1484

Anfossi D, Schayes G, Degrazia G, Goulart A (2004) Atmospheric turbulence decay during the solar total eclipse of 11 August 1999. Boundary-Layer Meteorol 111:301–311
Batchelor GK (1953) The theory of homogeneous turbulence. Cambridge University Press, Cambridge, 197 pp.
Biferale L, Boffeta G, Celani A, Lanotte A, Toschi F, Vergassola M (2003). The decay of homogeneous anisotropic turbulence. Phys Fluids 8:2105–2112
Caughey SJ, Kaimal JC (1977) Vertical heat flux in the convective boundary layer. Quart J Roy Meteorol Soc 103:811–815
Chasnov JR (1994) Similarity states of passive scalar transport in isotropic turbulence. Phys Fluids 6:1036–1051
Cole GS, Fernando HJS (1993) Some aspects of the decay of convective turbulence. Fluid Dyn Res 23:161–176
Cuijpers JWM, Duynkerke PG (1993) Large eddy simulation of trade wind cumulus clouds. J Atmos Sci 50:3894–3908
Cuijpers JWM, Holtslag AAM (1998) Impact of skewness and nonlocal effect on scalar and buoyancy fluxes in convective boundary layers. J Atmos Sci 55:151–162
Cuxart J, Morales G, Terradellas E, Yagüe C (2002) Study of coherent structures and estimation of the pressure transport terms for the nocturnal stable boundary layer. Boundary-Layer Meteorol 105:305–328
De Roode SR, Duynkerke PG, Jonker HJJ (2004) Large–eddy simulation: how large is large enough?. J Atmos Sci 61:403–421
Domaradzki JA, Rogallo RS (1989) Local energy transfer and nonlocal interactions in homogeneous, isotropic turbulence. Phys Fluids A 2:413–426
Dörnbrack A (1997) Broadening of convective cells. Quart J Roy Meteorol Soc 123:829–847
Fedorovich E, Nieuwstadt FTM, Kaiser R (2001) Numerical and laboratory study of a horizontally evolving convective boundary layer. Part II: effects of elevated wind shear and surface roughness. J Atmos Sci 58:546–560
Fitzjarrald DR, Freedman JM, Czikowsky MJ, Sakai RK, Acevedo OC, Moraes OLL (2004) Momentum and scalar transport during the decay of CBL Turbulence. Proceedings of the 16th conference on boundary layer and turbulence, Portland, ME, 2004
George WK (1992) The decay of homogeneous isotropic turbulence. Phys Fluids 4:1492–1509
Goulart A, Degrazia G, Rizza U, Anfossi D (2003) A theoretical model for the study of convective turbulence decay and comparison with large–eddy simulation data. Boundary-Layer Meteorol 107:143–155
Grant ALM (1997) An observational study of the evening transition boundary layer. Quart J Roy Meteorol Soc 123:657–677
Grimsdell AW, Angevine WM (2002) Observations of the afternoon transition of the convective boundary layer. J Appl Meteorol 41:3–11
Jonker HJJ, Vilà–Guerau de Arellano J (2005) The influence of chemistry on length scales of reactive species in convective atmospheric boundary layers. Khim Fiz 24(5):105–114
Jonker HJJ, Duynkerke PG, Cuijpers JWM (1999) Mesoscale fluctuations in scalars generated by boundary layer convection. J Atmos Sci 56:801–808
Jonker HJJ, Vilà–Guerau de Arellano J, Duynkerke PG (2004) Characteristic length scales of reactive species in a convective boundary layer. J Atmos Sci 61:41–56
Kaimal JC, Wyngaard JC, Haugen DA, Coté OR, Izumi Y, Caughey SJ, Readings CJ (1976) Turbulence structure in the convective boundary layer. J Atmos Sci 33:2152–2169
Monin AS, Yaglom AM (1975) Statistical fluid dynamics, vol 2 In: Lumley JL (ed) The MIT Press, Massachusetts, 874 pp.
Müller G, Chlond A (1996) Three-dimensional numerical study of cell broadening during cold-air outbreaks. Boundary-Layer Meteorol 81:289–323
Nieuwstadt FTM, Brost RA (1986) The decay of convective turbulence. J Atmos Sci 43:532–546
Pino D, Vilà–Guerau de Arellano J, Duynkerke PG (2003) Role of the shear in a convective boundary layer. J Atmos Sci 60:1913–1926
Pope SB (2000) Turbulent Flows. Cambridge University Press, Cambridge, 771 pp.
Shaw WJ, Barnard JC (2002) Direct numerical simulation decay. Proceedings of the 15th Conference on boundary layer and turbulence, 398–401, 2002
Skrbek L, Stalp SR (2000) On the decay of homogeneous isotropic turbulence. Phys Fluids 12:1997–2019
Sorbjan Z (1997) Decay of convective turbulence revisited. Boundary-Layer Meteorol 82:501–515
Stillinger DC, Helland KN, Van Atta CW (1983) Experiments on the transition of homogeneous turbulence to internal waves in a stratified fluid. J Fluid Mech 131:91–122

Stull RB (1988) An introduction to boundary layer meteorology. Kluwer Academic Press, Dordrecht, 666 pp.
Tennekes H, Lumley JL (1972) A first course in turbulence. The MIT Press, Massachusetts, 313 pp.
Tennekes H, Driedonks AGM (1981) Basic entrainment equations for the atmospheric boundary layer. Boundary-Layer Meteorol 20:515–531
Touil H, Bertoglio J-P, Shao L (2002) The decay of turbulence in a bounded domain. J Turbulence 3:049